# Determination of GaAs zinc blende/wurtzite band offsets utilizing GaAs nanowires with an axial GaAsSb insert

L. Ahtapodov, H. Kauko, A. M. Munshi, B. O. Fimland, A. T. J. van Helvoort, and H. Weman

Citation: Journal of Applied Physics **122**, 245102 (2017);
View online: https://doi.org/10.1063/1.4991884
View Table of Contents: http://aip.scitation.org/toc/jap/122/24
Published by the American Institute of Physics



# Determination of GaAs zinc blende/wurtzite band offsets utilizing GaAs nanowires with an axial GaAsSb insert

L. Ahtapodov,[1] H. Kauko,[2] A. M. Munshi,[1,3] B. O. Fimland,[1] A. T. J. van Helvoort,[2] and H. Weman[1]

[1]*Department of Electronic Systems, Norwegian University of Science and Technology (NTNU), NO-7491 Trondheim, Norway*

[2]*Department of Physics, Norwegian University of Science and Technology (NTNU), NO-7491 Trondheim, Norway*

[3]*CrayoNano AS, Sluppenvegen 6, NO-7037 Trondheim, Norway*

(Received 23 June 2017; accepted 9 December 2017; published online 26 December 2017)

By applying a correlated micro-photoluminescence spectroscopy and transmission electron microscopy (TEM) approach, we have utilized molecular beam epitaxy grown self-catalysed GaAs nanowires (NWs) with an axial GaAsSb insert to determine the band offsets at the crystal phase heterojunction between zinc blende (ZB) and wurtzite (WZ) GaAs. Two distinct PL emission bands originating from the ZB GaAsSb insert were identified. The lower energy PL emission allowed an independent verification of the maximum Sb molar fraction to be ~30%, in agreement with quantitative high-angle annular dark field scanning TEM performed on the same single NW. The higher energy PL emission revealed a low temperature ZB/WZ band offset of 120 meV at the interface between the two GaAs crystal phases occurring at the upper boundary of the insert. Separate conduction and valence band offsets develop at a higher temperature due to the different temperature dependence of the ZB and WZ GaAs band gaps, but both offset values show a relatively little variation in the range of 10–150 K. *Published by AIP Publishing*. https://doi.org/10.1063/1.4991884

## I. INTRODUCTION

The optical and electronic properties of the relatively newly emerged wurtzite (WZ) phase of most normally zinc blende (ZB) III-V semiconductor compounds, often observed in nanowires (NWs), have been the source of much controversy. Focusing on WZ GaAs, in particular, several historically significant studies have claimed values for the band gap in the range of 1.503–1.545 eV based on experimental[1–3] and theoretical[4,5] results. By direct correlation of micro-photoluminescence ($\mu$-PL) spectroscopy and transmission electron microscopy (TEM) on the same single NW, we established[6] the band gap of WZ GaAs at liquid He temperatures to be very similar to that of ZB GaAs, which is 1.52 eV.[7] This result has subsequently been verified independently in other works.[8,9] The corresponding band gap at room temperature (RT) is also debated, although it has received considerably less attention than the low-temperature (LT) band gap. In previous studies, we showed that the WZ GaAs band gap at RT is 1.444 eV,[6,8] whereas another study based on resonant Raman spectroscopy claimed 1.46 eV.[10] As the corresponding RT band gap of ZB GaAs is 1.425 eV,[7] both results indicate that the temperature dependence of the band gap differs between ZB and WZ GaAs. In fact, it cannot be ruled out that this difference is due to two different conduction bands participating in the PL transitions in WZ GaAs at LT ($\Gamma_8$) and RT ($\Gamma_7$). Due to the much lower oscillator strength of the dipole transition between the lower-lying $\Gamma_8$ conduction band and the valence band maximum,[3] the PL emission between these two bands would then only be observed at LT, whereas the $\Gamma_7$ conduction band will dominate at RT when it is thermally populated. If this is the case, the difference in the measured temperature dependence of the band gap between ZB and WZ GaAs will be due to the fact that PL spectroscopy does not determine the correct conduction band minimum ($\Gamma_8$) in WZ GaAs at RT. This question thus remains open, as the precise configuration of the WZ GaAs conduction bands as a function of temperature has, to the best of our knowledge, not been ascertained yet, neither theoretically nor experimentally.

It is well known that the crystal phase heterojunction between ZB and WZ GaAs occurring at crystallographic defects such as stacking faults (SF) and twin planes (TP) has a type-II band alignment with the WZ bands lying higher than the corresponding ZB bands.[11] However, the exact band offsets have long been an uncharted territory from an experimental point of view. Various works have reported SF- or TP-mediated emission in GaAs NWs at LT in the range 1.43 eV–1.50 eV, depending on the density of occurrence of the planar crystallographic defects.[11–13] Type-II transitions between electrons in bulk-like ZB GaAs and holes in bulk-like WZ GaAs have been assigned PL emission energies of 1.43 eV (Ref. 14) or 1.41–1.42 eV,[15] where the latter result is obtained with a combined PL and TEM approach similar to ours. Calculated band offsets reported in the literature fall in the range 79–122 meV for the valence band and 63–117 meV for the conduction band.[4,5] It should be pointed out that all theoretical models of the WZ GaAs band gap arrive at a different band gap width compared with ZB GaAs,[4,5] which is in contradiction with the most recent experimental evidence at LT.

## II. EXPERIMENTAL

### A. Nanowire growth

The NWs were grown by the self-catalysed vapor-liquid-solid technique on a Si(111) substrate using a Varian Gen II

Modular MBE system. The growth details are described elsewhere.[16] The NWs contain a single ~150–200 nm long axial GaAsSb insert and have a diameter of ~130 nm. In order to avoid the occurrence of a mixed ZB-WZ phase accompanying the solidification of the Ga droplet prior to and during the shell growth[17,18] and the possible effect of the shell on the core emission,[19] the NWs were not passivated by a radial shell as commonly done.

### B. Characterization

For the characterization, NWs were detached from the growth substrate and transferred onto a few-layer-graphene-coated Cu grid or 15 nm thick porous Si TEM substrates. The samples on graphene were studied with $\mu$-PL spectroscopy, quantitative high-angle annular dark-field (DF) scanning TEM (qHAADF-STEM) and energy-dispersive X-ray spectroscopy (EDX) on the same single NW in order to determine the Sb composition profile of the insert. The NWs on porous Si were investigated with correlated $\mu$-PL and conventional TEM, including selective area electron diffraction (SAED), dark-field (DF-) and high-resolution (HR-) TEM, on the same single NW.

## III. RESULTS AND DISCUSSION

### A. Structure and composition

All studied NWs exhibit a pure ZB crystal structure (including the GaAsSb insert) with occasional TPs below the GaAsSb insert. At the upper end of the insert, an atomically sharp transition to WZ crystal phase occurs, frequently accompanied by a couple of SFs or TPs in the close vicinity of the ZB/WZ interface. The WZ phase then normally continues for the rest of the NW growth, although it may switch to a mixed ZB/WZ phase at ~200 nm above the insert.[16,20] The characterization of the Sb composition of the insert with qHAADF-STEM has been described elsewhere,[21] whereby the present sample corresponds to growth batch "D" in that work. A steep build-up of the Sb composition in the axial direction is observed, until a plateau is reached near the centre of the insert. The plateau corresponds to the insert region with maximum Sb concentration, which was determined with qHAADF-STEM using a model that takes into account the radial out-diffusion of Sb atoms during the growth. Upon turning off the Sb flux, the Sb composition in the insert starts to decrease until the Ga droplet is depleted of Sb atoms, at which point the NW crystal structure switches to WZ. Due to the gradual decrease in the Sb content, we have defined the ZB/WZ interface as the upper boundary of the insert. Figure 1 introduces the structure of a representative NW labelled NW1, showing annular dark-field scanning TEM (ADF-STEM), axial composition profiles obtained with qHAADF-STEM (Sb) and EDX (Ga, As and Sb), and DF-TEM. There is a short axial ZB phase section with planar defects close to the ZB/WZ interface [solid blue line in Figs. 1(a)–1(c), green labeled in Fig. 1(c)], starting from the dashed blue line in Figs. 1(a)–1(c).

A HR-TEM image of the region around the ZB/WZ interface marked with a dashed yellow rectangle in Fig. 1(c),

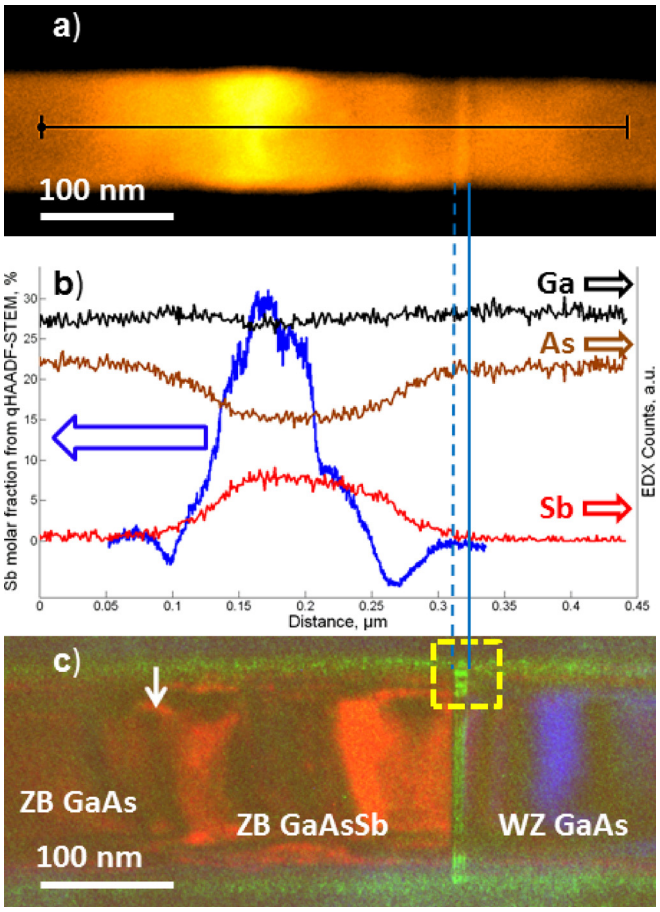


FIG. 1. (a) ADF-STEM image of NW1 around the GaAsSb insert region. The black line represents the EDX scan line corresponding to the black, brown and red composition profiles in (b). A pair of blue dashed and solid vertical lines mark the onset of a short region consisting of rotationally twinned ZB crystal phase (dashed line) and the ZB/WZ interface (solid line). The image is represented in false colors, and the brightness, contrast, and intensity histogram have been adjusted post-acquisition in order to enhance the visibility of the rotationally twinned region which serves as a marker. (b) Sb molar fraction profile determined with qHAADF-STEM (blue curve, left ordinate) and composition profiles for Ga (black), As (brown) and Sb (red) obtained from the EDX scan (right ordinate) corresponding to the black line in (a). (c) Composed DF-TEM image of the GaAsSb insert. The ZB crystal structure is shown in red and green (which is twinned relative to the phase depicted in red), and the WZ crystal structure corresponds to blue color. Red and green colors that can be seen inside the WZ region and outside the NW core are due to low signal in the individual DF images. A white arrow marks the lower end of the insert. Dashed yellow rectangle denotes the area imaged with HR-TEM in Fig. 2.

shown in Fig. 2 together with fast-Fourier transform (FFT) analysis of the crystal phases below (b), around (c), and above (d) the ZB/WZ interface, allows for a closer inspection of the NW segment with several random planar defects. From Fig. 2, it is evident that this region (marked with dashed and solid blue lines in Fig. 1 and dashed and solid blue arrows in Fig. 2) has a ZB crystal structure and contains five rotational TPs (marked with blue dashed and white arrows). According to the above definition of the upper boundary of the insert, this rotationally twinned NW segment lies within the insert. Furthermore, it is obvious from the Sb composition profiles obtained with qHAADF-STEM and EDX shown in Fig. 1(b) that this segment falls in a region

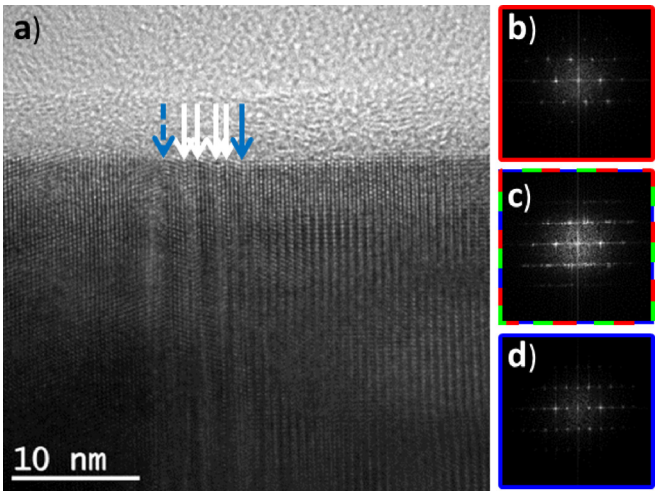


FIG. 2. (a) HR-TEM image of the region around the ZB/WZ interface in NW1 marked with a dashed yellow rectangle in Fig. 1(c). A dashed blue arrow marks the onset of a rotationally twinned ZB crystal phase region containing five TPs (marked with dashed blue and solid white arrows), and a solid blue arrow denotes the onset of the bulk-like WZ GaAs phase. (b)–(d) Fast-Fourier transform (FFT) analysis of the crystal phase (b) below the rotationally twinned region (ZB), (c) at the ZB/WZ interface, including the rotationally twinned region, and (d) above the ZB/WZ interface (WZ). The image borders in (b)–(d) are color-coded to correspond to the DF-TEM image in Fig. 1(c): red and green denote two different orientations of ZB crystal phase, and blue stands for WZ crystal phase. Red-green-blue dashed image border indicates the presence of both ZB orientations and WZ in the same region.

where the Sb composition has already decreased to zero and the insert material has fully evolved into pure GaAs. Thus, the upper boundary of the insert is in essence a boundary between ZB GaAs (below) and WZ GaAs (above).

### B. Energy band alignment of the GaAsSb insert

The LT (15 K) $\mu$-PL spectra of the studied NWs consist of two emission bands which will be discussed consecutively in the following: a group of two peaks around 1 eV and a single or double peak at ~1.40 eV. Figure 3(a) shows the $\mu$-PL spectrum of the 1 eV emission region of NW1. Our model for the Sb composition profile of the insert is presented in Fig. 3(b), and the resulting electronic band diagram of the region around the insert is sketched in Fig. 3(c).

There are two relatively broad emission peaks in the 1 eV region: one at 1 eV and another at 1.03 eV. The higher-energy peak (1.03–1.04 eV) shows a considerable blue shift with excitation power (not shown), and at higher excitation power, the lower-energy peak is completely suppressed by it. This indicates that the 1 eV peak is due to a less probable, possibly spatially indirect transition, whereas the emission at 1.03 eV corresponds to a more probable recombination route which involves a greater number of electronic states, possibly around the centre of the insert.

The Sb composition profile of the $GaAs_{1-y}Sb_y$ insert has been obtained with qHAADF-STEM [Fig. 1(b)], and it peaks at an Sb molar fraction of $y = 0.30$. This provides an accurate result for the maximum Sb composition at the centre of the insert. However, at the interfaces of the insert with the NW segments below and above it and at lattice defects, the HAADF-STEM intensity variation is mainly governed by dechanneling rather than compositional changes which causes an unphysical negative dip in the Sb-profile[21] [Fig. 1(b), dips centered around ~0.1 $\mu$m and ~0.26 $\mu$m]. EDX line scans can visualize better the Sb-profile at the interfaces, albeit the accuracy of the compositional analysis and the spatial resolution are much poorer than for qHAADF-STEM.[21] Thus, the qHAADF-STEM maximum molar fraction of $y = 0.30$ reported earlier for this NW was used to construct the band alignment model of the insert presented in Fig. 3(c). It is well known that the Sb composition of the insert is governed by diffusion of Sb atoms into the Ga droplet and diffusion into the NW from the Ga droplet. Hence, it is expected to rise steeply until a maximum Sb composition is reached at the centre of the insert. Depleting the droplet of Sb atoms is a different process and it proceeds exponentially. This behavior has previously been observed for GaAsSb inserts[21–23] and other III-V inserts[24] in both Au- and Ga-assisted GaAs NWs and is sketched for the here-studied GaAsSb insert in Fig. 3(b).

The band alignment between ZB GaAs and ZB $GaAs_{1-y}Sb_y$ has been found to be type-I within the entire range of Sb molar fractions $y$ discussed here (0–0.30).[25–27] However, as the Sb molar fraction increases from 0 at the lower end of the insert to 0.30 near the centre, the offset of the GaAsSb conduction band to the ZB GaAs conduction band passes through a minimum at around $y = 0.20$ before it reaches a local maximum as the composition nears the type-I/type-II crossover point at $y \sim 0.34$.[25] The same behavior is observed (in reverse order) as the Sb molar fraction decreases again toward the upper end of the insert, although the conduction band profile is different due to the more gradual profile of the Sb composition. Thus, the conduction band forms an asymmetric W-type potential. The valence band profile was then calculated by using the empirical GaAsSb band gap model represented by formula 6 in Ref. 28 to determine the band gap, and then by subtracting the appropriate band gap width from the already determined GaAsSb conduction band profile. Unlike the conduction band, the valence band edge of the insert rises monotonously toward the region of maximum Sb molar fraction and drops continuously as the material turns into pure GaAs. The practical procedure for modelling the GaAsSb insert band alignment is summarized below and the entire band diagram is presented in Fig. 3(c), together with arrows corresponding to the observed optical recombination paths:

Firstly, the Sb composition in the lower part of the GaAsSb insert (90 nm) is modelled as $1 - erf(x)$, and in the upper part (150 nm), as $exp(-x)$ where $x$ represents the distance along the NW axis. For the peak Sb molar fraction, a value of 0.30 was adopted following the qHAADF-STEM results. Next, the Sb composition-dependent GaAsSb conduction band edge offset to ZB GaAs is reconstructed after Fig. 3 in Ref. 25 and the offset profile is calculated for each point in the Sb composition profile as obtained in the previous step. After that, the GaAsSb band gap is computed for each point in the conduction band edge offset profile using Formula 6 in Ref. 28. Then the GaAsSb band gap profile as obtained in the previous step is subtracted from the GaAsSb

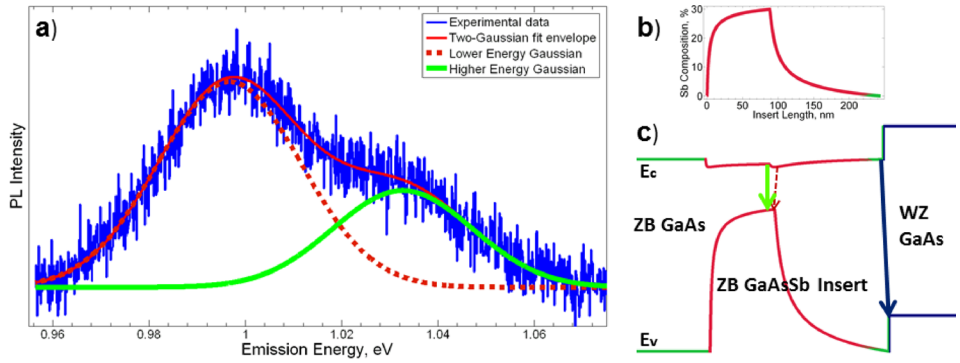


FIG. 3. (a) Low excitation power PL spectrum of NW1 showing the 1 eV emission region. Solid red line corresponds to a two-Gaussian lineshape fit that was employed for the purpose of precise determination of the emission energy. The two Gaussian components are also indicated with dashed red (1 eV peak) and solid green (1.03 eV peak) lines. (b) Schematic variation of the Sb molar fraction along the GaAsSb insert due to build-up and depletion of Sb in the Ga catalyst droplet. (c) Band alignment model for the insert with the GaAsSb insert depicted in red, ZB GaAs in green, and WZ GaAs in blue. The valence and conduction bands are separately drawn to scale. The color in the Sb composition profile in (b) and the band diagram of the insert in (c) changes from red to green towards the upper boundary of the insert in order to reflect the transition of the insert material from GaAsSb to GaAs. The dashed red arrow in (c) denotes an optical recombination corresponding to the 1 eV PL peak in (a), whereas the solid green arrow corresponds to the ~1.03 eV PL emission. A solid blue arrow represents the type-II PL emission between electrons in the ZB and holes in the WZ GaAs phases.

conduction band edge profile in order to obtain the valence band profile of the insert. Finally, the WZ GaAs band gap above the insert is taken to be the same as the ZB GaAs band gap and the ZB/WZ band offset in Fig. 3(c) is initially taken to be 110 meV after Ref. 15. Following the data analysis in the present study, the offset was later re-adjusted to 120 meV.

The $\mu$-PL spectrum of Fig. 3(a) can be interpreted as follows. The weak emission at 1 eV corresponds to spatially indirect transitions between the upper minimum of the W-potential well in the conduction band and the valence band potential well near the centre of the insert [shown with a dashed red arrow in Fig. 3(c)]. Both minima of the W-potential are wide and shallow which explains why no signs of quantum confinement were observed in the PL spectra. However, the left minimum (physically closer to the lower end of the insert) is too far from the maximum of the valence band and is hence unlikely to contribute any PL emission. The more prominent emission at 1.03 eV [green arrow in Fig. 3(c)], which gains in intensity and dominates the 1 eV emission region at all but the lowest excitation powers, is assigned to spatially direct recombination of higher-lying electrons with holes close to the centre of the insert which will become a more favorable recombination route when excitation power-induced band filling takes place. The above reasoning justifies choosing the 1.03 eV peak for the optical determination of the maximum Sb molar fraction within the insert.[23] Its emission energy was inferred from a Gaussian fit to the peak at an excitation level where it is just resolvable, in order to prevent the peak energy from being affected by any band filling-related blue shift at higher excitation [green Gaussian curve fit in Fig. 3(a)]. Using data from all studied NWs, an average maximum Sb molar fraction of $y = 0.28 \pm 0.01$ was calculated following formula 6 in Ref. 28. For the specific NW1, $y = 0.29$ was obtained, which is in good agreement with the value of $y = 0.30$ for the Sb molar fraction near the centre of the insert determined with qHAADF-STEM. Furthermore, the difference in the emission energy between the PL originating from the broader W-well minimum and the 1.03 eV peak amounts to 32 meV, which is in agreement with the GaAsSb conduction band model presented by Johnson *et al.*[25]

### C. ZB/WZ GaAs band offsets

Apart from explaining the $\mu$-PL spectra of the studied NWs in the 1 eV energy region, the band diagram in Fig. 3(c) opens up for the interesting prospect of using the present NW structure as a platform for observing the PL signal due to a recombination between electrons at the energy of the ZB GaAs phase conduction band at the upper boundary of the insert and holes in the WZ GaAs continuum above the insert, depicted with a blue arrow in Fig. 3(c). All studied NWs exhibited an additional PL band at higher energy, found to be in the range 1.385–1.41 eV. The excitation power-dependent PL spectra from a typical example NW, labelled NW2, are shown in Fig. 4(a) together with the corresponding structural TEM data of the insert in Figs. 4(b)–4(f). The excitation power dependence of the PL emission exhibits a gradual blue shift at a higher excitation power but no signs of quantum confinement were observed. The structural analysis by TEM confirms that the insert has a pure ZB crystal phase and shows that the transition to the extended region of WZ GaAs above the insert is atomically sharp. One isolated TP is present in the ZB GaAs phase in the immediate vicinity of the crystal phase heterojunction. It is, however, unlikely to yield a contribution to the PL spectra in this energy range.[13] Hence, we reason that the $\mu$-PL emission in the region 1.38–1.41 eV is due to recombination of electrons in the ZB GaAsSb phase of exponentially decreasing Sb composition at the upper end of the insert with holes in the WZ GaAs phase at low excitation. As the excitation power is increased and the PL peak is blue shifted due to band filling inside the insert, the PL emission will effectively represent the spatially indirect optical recombination between electrons in ZB GaAs and holes in WZ GaAs. The PL emission energy corresponding to the largest blue shift can therefore be used to

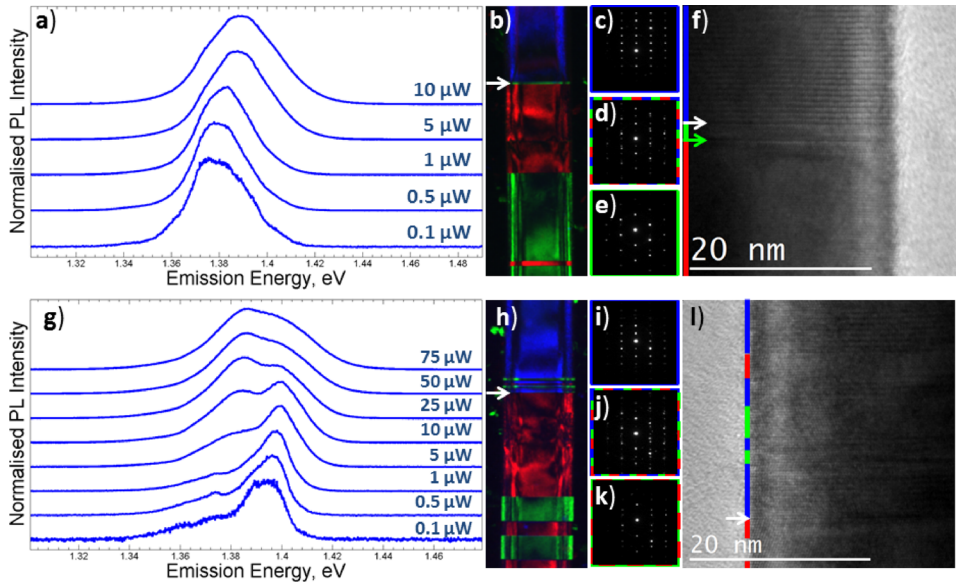


FIG. 4. (a) Excitation power-dependent PL spectra of the 1.4 eV region for NW2, normalized to the peak intensity. The structural properties of NW2 are shown in (b)–(f) where the color coding is the same as in Figs. 1 and 2. The upper end of the GaAsSb insert is marked with a white arrow in (b) and in the HR-TEM image in (f). Above it, the NW consists of SF-free WZ GaAs crystal phase as illustrated by the SAED pattern in (c). Below, the crystal phase of the GaAsSb insert is ZB [see SAED pattern in (e)], with one isolated SF (green arrow) within the green labelled ZB section. The SAED pattern in (d) was taken from the region around the ZB/WZ interface and hence contains both the ZB and WZ diffraction peaks. (g) Normalized excitation power-dependent PL spectra from NW3. The crystal structure of NW3 is presented in (h)–(l) by DF-TEM (h), SAED above (i), around (j), and below (k) the ZB/WZ interface and HR-TEM (l) images, respectively. NW3 contains several ZB segments in the WZ phase above the insert, close to the ZB/WZ interface, which are indicated with a color bar in the HR-TEM image in (l).

arrive at an estimate for the band offsets at the crystal phase heterojunction between ZB and WZ GaAs. The practical procedure for this is outlined below.

The energy of the indirect optical recombination of electrons in the ZB GaAs with holes in the WZ GaAs was determined for all NWs by fitting the PL emission with a Gaussian lineshape function and selecting the most blue shifted one which corresponds to the strongest band filling inside the GaAsSb insert. The energy of the type-II transition was then averaged between all studied NWs and the value obtained for the standard deviation was adopted as the error margin in the subsequent band offset determination. The valence band offset between ZB and WZ GaAs was obtained by subtracting the energy of the type-II transition from the ZB GaAs band gap (1.52 eV).[7] The conduction band offset between ZB and WZ GaAs was obtained analogously to the valence band offset; however, now, the energy of the type-II transition was subtracted from the sum of the WZ GaAs free exciton emission energy[6] and the ZB GaAs free exciton binding energy (4.3 meV).

For the type-II optical recombination of electrons in the ZB GaAs phase at the upper end of the insert with holes in the WZ GaAs above it, a mean emission energy of 1.396 eV with a standard deviation of 22 meV was obtained. Since the ZB and WZ GaAs band gaps at LT are the same,[6] the LT conduction and valence band offsets are both equal to $120 \pm 11$ meV, which is in reasonable agreement with the corresponding value of 100–110 meV reported previously for GaAs NWs grown by metal-organic vapor phase epitaxy (MOVPE).[15] However, we note that it is possible that the conduction band offset is underestimated by a few meV by our method due to the possibility that the WZ GaAs conduction band has $\Gamma_8$ symmetry which has a larger electron effective mass.

The correlated $\mu$-PL-TEM data from another NW, NW3, presented in Figs. 4(g)–4(l), further support the analysis presented so far. The structural information for NW3 obtained with HR-TEM [Fig. 4(l)] indicates the presence of several short ZB segments in the WZ GaAs phase above and in the immediate vicinity of the upper interface of the insert. Correspondingly, the excitation power-dependent PL spectra from NW3 [Fig. 4(g)] contain an emission peak at a higher energy (1.396 eV), which dominates the spectra at a low excitation power but is completely suppressed at higher excitation by the PL emission due to the recombination of "hot" electrons inside the GaAsSb insert with holes in the WZ GaAs above it, as discussed in relation to Fig. 4(a), which is at 1.386 eV for NW3. As it is very unusual for a higher-energy PL peak to be dominated by a lower-energy PL peak at high excitation power, we conclude that this emission originates from quantum confined electrons at the crystallographic defects in the WZ GaAs phase above the GaAsSb insert which will lie higher in energy than the insert conduction band edge, and holes inside the WZ GaAs. The weaker intensity compared with the bulk-like type-II emission at high excitation power is explained by the smaller number of states available for electrons trapped at the defects. It must be mentioned that other NWs that switch from WZ GaAs above the insert to a mixed ZB/WZ GaAs phase further up along the NW (~200 nm above the insert) do not exhibit any shoulder lines to the main emission spectra at 1.385–1.411 eV. This is, however, not surprising as bare-core GaAs NWs grown at identical conditions but without an insert did not yield any PL signal at all due to the detrimental effects of surface states.

The temperature dependence of the ZB/WZ GaAs valence and conduction band offsets up to 150 K is shown in Fig. 5. For these calculations, the same procedure as outlined above is used. The temperature-dependent emission energy of the type-II PL transition (not shown), which is at 1.38–1.41 eV at LT, is now subtracted from the correct ZB or WZ GaAs band gap at the corresponding temperature. The temperature dependence of the ZB and WZ GaAs band gap was taken from Refs. 7 and 6, respectively. Inasmuch as the cited temperature dependence of the WZ GaAs band gap was measured with $\mu$-PL, it is important to point out explicitly that we have assumed the same conduction band (i.e., $\Gamma_7$, following prevailing experimental evidence[3]) to be responsible for the PL emission from WZ GaAs in the range 10–150 K.

It is evident that the band offsets depend very weakly on the temperature, whereby the mean values remain between 120 and 130 meV throughout the studied temperature range. Furthermore, although one can use a single value for the band offsets at low T and up to 50 K, separate valence and conduction band offsets begin to develop at higher temperatures due to the inherently different temperature behavior of the band gap for ZB and WZ GaAs phases.[6] This will also be true at RT where the WZ GaAs band gap is larger than the ZB GaAs band gap.[6,8,9]

## IV. CONCLUSION

In conclusion, we have studied multiple self-catalysed GaAs NWs with an axial $GaAs_{1-y}Sb_y$ insert by correlated $\mu$-PL and TEM. The NW structure was found to be ZB below and within the insert and WZ above it, with two PL emission regions centred around 1 eV and just below 1.4 eV, respectively. The present results for the Sb composition expressed in terms of the Sb molar fraction determined from the $\mu$-PL emission energy in the 1 eV range provide an independent verification of the method for determining the maximum Sb molar fraction with quantitative HAADF-STEM, as both methods yield a maximum Sb molar fraction of $y = 0.29$–$0.30$. The gradual decrease in the Sb molar fraction above the centre of the insert leads to the formation of a ZB/WZ GaAs crystal phase heterojunction at its upper boundary. At $1.396 \pm 0.011$ eV, a type-II PL emission due to the recombination of electrons in the ZB with holes in the WZ GaAs crystal phase was observed. This enabled us to determine the conduction and valence band offsets for the ZB/WZ GaAs crystal phase heterojunction to be $120 \pm 11$ meV at LT, and to show a relatively weak temperature dependence up to 150 K.

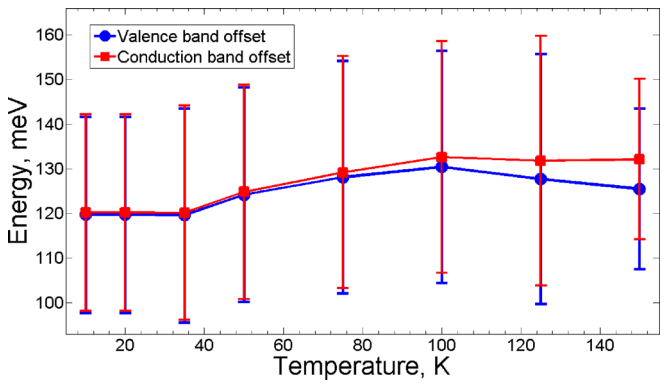


FIG. 5. Temperature dependence of the conduction (red) and valence (blue) band offsets between ZB and WZ GaAs.

## ACKNOWLEDGMENTS

The authors would like to thank Dr. Dingding Ren for his valuable inputs in the discussion of the present results. The Research Council of Norway is acknowledged for the support from the FRINATEK program (Grant No. 214235), NANO2021 program (Grant No. 239206), and the NORTEM project (Grant No. 197405).

[1]T. B. Hoang, A. F. Moses, H. L. Zhou, D. L. Dheeraj, B. O. Fimland, and H. Weman, Appl. Phys. Lett. **94**(13), 133105 (2009).
[2]S. Breuer, C. Pfüller, T. Flissikowski, O. Brandt, H. T. Grahn, L. Geelhaar, and H. Riechert, Nano Lett. **11**(3), 1276 (2011).
[3]B. Ketterer, M. Heiss, E. Uccelli, J. Arbiol, and A. Fontcuberta i Morral, ACS Nano **5**(9), 7585 (2011).
[4]M. Murayama and T. Nakayama, Phys. Rev. B **49**(7), 4710 (1994).
[5]A. De and C. E. Pryor, Phys. Rev. B **81**(15), 155210 (2010).
[6]L. Ahtapodov, J. Todorovic, P. Olk, T. Mjåland, P. Slåttnes, D. L. Dheeraj, A. T. J. van Helvoort, B. O. Fimland, and H. Weman, Nano Lett. **12**(12), 6090 (2012).
[7]P. Lautenschlager, M. Garriga, S. Logothetidis, and M. Cardona, Phys. Rev. B **35**(17), 9174 (1987).
[8]D. C. Kim, D. L. Dheeraj, B. O. Fimland, and H. Weman, Appl. Phys. Lett. **102**(14), 142107 (2013).
[9]S. Furthmeier, F. Dirnberger, J. Hubmann, B. Bauer, T. Korn, C. Schüller, J. Zweck, E. Reiger, and D. Bougeard, Appl. Phys. Lett. **105**(22), 222109 (2014).
[10]P. Kusch, S. Breuer, M. Ramsteiner, L. Geelhaar, H. Riechert, and S. Reich, Phys. Rev. B **86**(7), 075317 (2012).
[11]D. Spirkoska, A. L. Efros, W. R. L. Lambrecht, T. Cheiwchanchamnangij, A. Fontcuberta i Morral, and G. Abstreiter, Phys. Rev. B **85**(4), 045309 (2012).
[12]M. Heiss, S. Conesa-Boj, J. Ren, H. H. Tseng, A. Gali, A. Rudolph, E. Uccelli, F. Peiró, J. R. Morante, D. Schuh, E. Reiger, E. Kaxiras, J. Arbiol, and A. Fontcuberta i Morral, Phys. Rev. B **83**(4), 045303 (2011).
[13]N. Vainorius, S. Lehmann, D. Jacobsson, L. Samuelson, K. A. Dick, and M. E. Pistol, Nano Lett. **15**(4), 2652 (2015).
[14]D. Spirkoska, J. Arbiol, A. Gustafsson, S. Conesa-Boj, F. Glas, I. Zardo, M. Heigoldt, M. H. Gass, A. L. Bleloch, S. Estrade, M. Kaniber, J. Rossler, F. Peiro, J. R. Morante, G. Abstreiter, L. Samuelson, and A. Fontcuberta i Morral, Phys. Rev. B **80**(24), 245325 (2009).
[15]N. Vainorius, D. Jacobsson, S. Lehmann, A. Gustafsson, K. A. Dick, L. Samuelson, and M. E. Pistol, Phys. Rev. B **89**(16), 165423 (2014).
[16]A. M. Munshi, D. L. Dheeraj, J. Todorovic, A. T. J. van Helvoort, H. Weman, and B. O. Fimland, J. Cryst. Growth **372**, 163 (2013).
[17]L. Ahtapodov, A. M. Munshi, J. S. Nilsen, J. F. Reinertsen, D. L. Dheeraj, B. O. Fimland, A. T. J. van Helvoort, and H. Weman, Nanotechnology **27**(44), 445711 (2016).
[18]X. Yu, H. Wang, J. Lu, J. Zhao, J. Misuraca, P. Xiong, and S. von Molnár, Nano Lett. **12**(10), 5436 (2012).
[19]R. Songmuang, L. T. T. Giang, J. Bleuse, M. Den Hertog, Y. M. Niquet, L. S. Dang, and H. Mariette, Nano Lett. **16**(6), 3426 (2016).
[20]D. Ren, D. L. Dheeraj, C. Jin, J. S. Nilsen, J. Huh, J. F. Reinertsen, A. M. Munshi, A. Gustafsson, A. T. J. van Helvoort, H. Weman, and B. O. Fimland, Nano Lett. **16**(2), 1201 (2016).
[21]H. Kauko, B. O. Fimland, T. Grieb, A. M. Munshi, K. Müller, A. Rosenauer, and A. T. J. van Helvoort, J. Appl. Phys. **116**(14), 144303 (2014).
[22]H. Kauko, T. Grieb, R. Bjørge, M. Schowalter, A. M. Munshi, H. Weman, A. Rosenauer, and A. T. J. van Helvoort, Micron **44**, 254 (2013).
[23]J. Todorovic, H. Kauko, L. Ahtapodov, A. F. Moses, P. Olk, D. L. Dheeraj, B. O. Fimland, H. Weman, and A. T. J. van Helvoort, Semicond. Sci. Technol. **28**(11), 115004 (2013).
[24]V. G. Dubrovskii and N. V. Sibirev, Cryst. Growth Des. **16**(4), 2019 (2016).

[25]S. R. Johnson, C. Z. Guo, S. Chaparro, Y. G. Sadofyev, J. Wang, Y. Cao, N. Samal, J. Xu, S. Q. Yu, D. Ding, and Y. H. Zhang, J. Cryst. Growth **251**(1–4), 521 (2003).
[26]J. B. Wang, S. R. Johnson, S. A. Chaparro, D. Ding, Y. Cao, Y. G. Sadofyev, Y. H. Zhang, J. A. Gupta, and C. Z. Guo, Phys. Rev. B **70**(19), 195339 (2004).
[27]T. Xu, M. J. Wei, P. Capiod, A. Díaz Álvarez, X. L. Han, D. Troadec, J. P. Nys, M. Berthe, I. Lefebvre, G. Patriarche, S. R. Plissard, P. Caroff, P. Ebert, and B. Grandidier, Appl. Phys. Lett. **107**(11), 112102 (2015).
[28]R. Teissier, D. Sicault, J. C. Harmand, G. Ungaro, G. Le Roux, and L. Largeau, J. Appl. Phys. **89**(10), 5473 (2001).